THE ASTROPHYSICAL JOURNAL, 452:275–285, 1995 October 10

ATOMIC PHYSICS WITH THE GODDARD HIGH-RESOLUTION SPECTROGRAPH ON THE *HUBBLE SPACE TELESCOPE*. II. OSCILLATOR STRENGTHS FOR SINGLY IONIZED IRON[1]

JASON A. CARDELLI
Department of Astronomy and Astrophysics, Villanova University, Villanova, PA 19085,[2] and Department of Astronomy, University of Wisconsin, Madison

AND

BLAIR D. SAVAGE
Department of Astronomy, University of Wisconsin, Madison, WI 53706
Received 1995 January 9; accepted 1995 April 20

ABSTRACT

Moderate-to-high signal-to-noise interstellar absorption line data, obtained with the Goddard High-Resolution Spectrograph aboard the *Hubble Space Telescope* toward β^1 Sco, HD 18100, and μ Col, are used to derive absolute oscillator strengths (f-values) for a number of weak and strong ultraviolet resonance transitions of Fe II spanning a range of line absorption strengths (i.e., the product of f-value and wavelength, $f\lambda$) of over a factor 4000. Included in the list of lines seen in the spectrum of β^1 Sco are $4s\ ^6D_{9/2}$–$y\ ^4F^o_{7/2}$ λ1611.2 ($W_\lambda = 12.8 \pm 1.1$ mÅ) and the first known interstellar detection of the weak transition $4s\ ^6D_{9/2}$–$z\ ^6F^o_{7/2}$ λ2367.6 ($W_\lambda = 2.0 \pm 0.3$ mÅ). The new f-values, which carry absolute 1 σ uncertainties of 7%–18%, are referenced to the results obtained from a detailed analysis of the moderately weak transitions $4s\ ^6D_{9/2}$–$z\ ^4D^o_{7/2}$ λ2249.9 and $4s\ ^6D_{9/2}$–$z\ ^4F^o_{9/2}$ λ2260.8 using the recent well-measured ($\pm$8%) laboratory f-values of Bergeson, Mullman, & Lawler (1994). For the ultraviolet transitions studied here, the large range of absorption strengths provides the opportunity for *self-consistent* analyses of ISM Fe II abundances over a large dynamic range (e.g., between different sight lines sampling a large range of column densities or in single sight lines with multiple and widely varying component structure). For example, application of these new f-values to the Fe II transitions observed toward β^1 Sco enables us to trace variations of the column density of Fe II with velocity to a sensitivity of better than 1 part in 10,000.

Subject headings: atomic processes — ISM: abundances — ultraviolet: ISM

1. INTRODUCTION

In recent years, spectroscopic studies of the interstellar medium (ISM) have been greatly aided through substantial improvements in both ground- and space-based instrumentation. For example, with moderate-resolution (15 km s^{-1}) and high-resolution (3.5 km s^{-1}) gratings and the capability to produce high signal-to-noise ratio (S/N > 100/1) photon-limited data, the Goddard High-Resolution Spectrograph (GHRS) aboard the *Hubble Space Telescope* (*HST*) has produced UV data of unprecedented quality (Savage, Cardelli, & Sofia 1992; Federman et al. 1993; Cardelli et al. 1993b, c, 1994; Fitzpatrick & Spitzer 1994; Lambert et al. 1994). Even at modest S/N values (50/1), GHRS absorption-line measurement errors are routinely smaller than 5%. Such small measurement errors are particularly significant in cases of high-dispersion echelle mode observations of weak lines ($W_\lambda < 10$–15 mÅ), in which corrections for absorption-line saturation are relatively small or negligible and from which accurate abundances can be derived. In a growing number of cases, the inferred accuracy of the derived abundances far exceeds the accuracy of the available atomic data (e.g., f-values; see Morton 1991, hereafter M91).

The situation has been improving recently with the availability of new laboratory lifetime and branching ratio measures for a number of observable UV transitions for important atomic species. These data then allow determinations of f-values. For example, reliable experimental f-values are now available for C II] λ2325 (Fang et al. 1993), Si II] λ2335 (Calamai, Smith, & Bergeson 1993), Si II λ1808 (Bergeson & Lawler 1993a), Cr II $\lambda\lambda$2056, 2062, 2066 and Zn II $\lambda\lambda$2026, 2062 (Bergeson & Lawler 1993b), and Fe II $\lambda\lambda$2249, 2260 (Bergeson et al. 1994). These atomic species are particularly important since they serve as principal components of, and diagnostics for, such things as molecule formation, dust chemistry, and Galactic and extragalactic chemical evolution.

Unfortunately, for some species for which numerous observable UV transitions exist, the question of reliability of their f-values (M91) presents potentially serious problems. For example, comparisons made between analyses that rely on abundances derived from *different* transitions of the same species can lead to serious errors in interpretation. Since there will always be circumstances where transitions different from those listed above must be used (e.g., restricted wavelength coverage and/or line strength requirements), reliable and self-consistent atomic data for a range of transitions are needed.

In this paper, we explore the reliability of a number of transitions of Fe II covering a range in wavelength from 1140 to 2600 Å and a range of absorption strengths ($f\lambda$) of over a factor 4000. The data correspond to Fe II absorption-line measures obtained with the GHRS toward three stars probing widely varying ISM characteristics (i.e., total column density, component structure, and gas-phase conditions). The analysis centers on using observations of Fe II $\lambda\lambda$2249 and 2260 to establish accurate absolute column densities to which the other

[1] Based on observations obtained with the NASA/ESA *Hubble Space Telescope* through the Space Telescope Science Institute, which is operated by the Association of Universities for Research in Astronomy, Inc., under NASA contract NASA-26555.

[2] Permanent address.

transitions are compared. Where possible, the analyses of transitions in common between the different sight lines are cross-checked so as ensure self-consistent results.

2. OBSERVATIONAL DATA

The Fe II data discussed here represent a subset of data obtained with the GHRS aboard *HST* from two separate and distinct ISM absorption-line programs designed to study (1) the gas and dust characteristics in a local ($d = 160$ pc) diffuse molecular cloud (β^1 Sco) and (2) the abundance and distribution of low and high ions in a long path length ($d = 3100$ pc), low-density sight line into the halo (HD 18100, $z = -2800$ pc; see Savage & Sembach 1994). For β^1 Sco, the observations (obtained in 1993 August) include the resonance transitions Fe II $\lambda\lambda$1142 and 1611 observed with the medium-resolution grating G160M (15 km s^{-1}) and $\lambda\lambda$2249, 2367, 2374, and 2600 observed with the high-resolution echelle B grating (3.5 km s^{-1}). For HD 18100, the observations (obtained in 1992 October) include the transitions of Fe II $\lambda\lambda$2260, 2374, and 2600 observed with echelle B.

Also included in our analysis are data of μ Col, a lightly reddened, bright O star observed as a GHRS calibration standard. The star μ Col is a runaway halo star ($d = 1068$ pc) sampling relatively low-density diffuse gas (see Sofia, Savage, & Cardelli 1993). The path to μ Col shares characteristics similar to the HD 18100 sight line. The data, obtained during 1994 (since the refurbishment of *HST* and restoration of the GHRS side 1 echelle A grating), include the transitions of Fe II $\lambda\lambda$1608, 1611, 2249, 2260, 2344, 2374, 2382, 2586, and 2600 obtained with echelle A and B. Basic data on the three stellar sources and sight lines are given in Table 1.

The observations for β^1 Sco and HD 18100 were obtained with the stellar images positioned in the small (0".25 × 0".25) science aperture (SSA). Since these data were obtained prior to the *HST* refurbishment and installation of the COSTAR corrective optics payload, the SSA was used to preserve spectral resolution. Details regarding the characteristics of the GHRS can be found in Duncan & Ebbets (1990) and Brandt et al. (1994). The exposures were acquired using a data sampling strategy corresponding to two samples per diode (STEP-PATT = 4 and 6 for G160M and echelle B, respectively). Observations at each primary wavelength consisted of exposures utilizing the FP-SPLIT = 4 procedure to reduce the effects of fixed-pattern noise and photocathode granularity present in the Digicon detectors. This procedure consists of breaking each observation into a set of four subexposures, each obtained at a slightly different grating carousel position (details of the noise removal procedures can be found in Cardelli & Ebbets 1994; Cardelli et al. 1994; and Fitzpatrick & Spitzer 1994).

The calibration data of μ Col were all obtained with the large (2".0 × 2".0) science aperture (LSA) and sampling strategies including both two and four samples per diode (STEP-PATT = 6 and 7, respectively, for echelle A and B). Since these data were obtained after the installation of COSTAR, the point-spread function seen through the LSA has been corrected for the effects of spherical aberration produced by the primary mirror. Also, because these data were obtained as part of an extensive multiwavelength scanning calibration program (resolution and throughput), they were not obtained with the command FP-SPLIT and so cannot be processed for fixed-pattern noise removal as the data for the other targets were. However, in several cases, multiple observations from different calibration runs obtained at slightly different central wavelengths were available for which some noise assessment was possible.

We followed the data reduction procedure of Cardelli et al. (1991) and Savage et al. (1992) for data extraction, background processing and subtraction, and wavelength calibration of the data. The basic raw data reduction was performed using the package CALHRS at the GHRS computing facility at the Goddard Space Flight Center (CALHRS is also part of the standard Space Telescope Science Institute pipeline and IRAF reduction packages). This includes conversion to count rates, correcting for particle radiation, dark counts, diode nonuniformities, paired pulse events (where applicable), and wavelength calibration using the standard calibration tables available at the Space Telescope Science Institute. The final data reduction, which includes background subtraction, fixed-pattern/granularity noise extraction and removal, and merging of the individual FP-SPLIT subexposures, was performed using software developed and tested at the University of Wisconsin, Madison. A second-order scattered light correction was applied to the echelle data according to the prescription outlined in Cardelli, Ebbets, & Savage (1990, 1993a).

Line profiles for the Fe II data obtained with the high-resolution echelle gratings, normalized to unity continuum and plotted against heliocentric velocity, $v_{\rm helio}$, are shown in Figures 1, 2, and 3 for β^1 Sco, HD 18100, and μ Col, respectively. Also shown in the figures are the measured continuum S/N values and the total integrated equivalent widths. The β^1 Sco data for Fe II λ2367 represent the first known interstellar detection of this weak transition. The equivalent width measures for the entire ensemble of data analyzed here are summarized in Table 2 along with the 1 σ uncertainties (see Cardelli et al. 1991 for a discussion of the error derivation).

TABLE 1

BASIC STELLAR TARGET AND SIGHT LINE DATA

Star	Spectral Type	l^a	b^a	Distance (pc)	log $N(H_{total})^b$	$\langle n \rangle^c$
β^1 Sco	B0.5 V	350°	23°	160	21.14	2.80
HD 18100...	B1 V	218	−63	3100	20.14	0.014
μ Col	O9.5 V	237	−27	1068	19.85	0.021

[a] Galactic longitude (l) and latitude (b).

[b] Logarithm of the column density of hydrogen nuclei, including contributions from H I and H_2 only. Contribution from ionized gas (H II) could be as high as 20% of the total for μ Col and HD 18100.

[c] Mean sight-line density (cm^{-3}) defined as N(H)/distance.

3. ANALYSIS

3.1. *Methodology and Baseline Data*

In order to derive absolute f-values for the Fe II resonance transitions studied here, the analysis requires that we baseline against some adopted f-value reference standard. For this purpose we use the Fe II transitions $\lambda\lambda$2249 and 2260, for which reliable laboratory f-values exist (Bergeson et al. 1994). These f-values have a 1 σ uncertainty of 8% and were obtained by combining accurate measures of branching ratios with accurate values of the radiative lifetime of the upper states. The basic atomic data for these two transitions are given in Table 3. In the discussion that follows, we outline the procedures we used to determine the Fe II column densities from these tran-

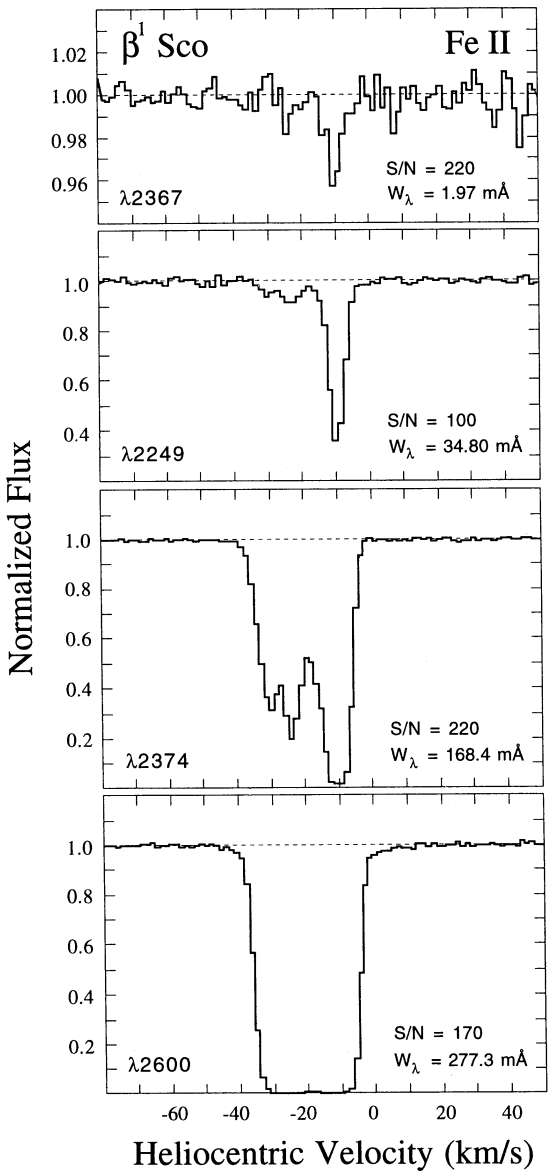

FIG. 1.—Continuum normalized absorption-line intensities plotted against heliocentric velocity for Fe II lines observed with the echelle B grating (3.5 km s^{-1} resolution) in the sight line to β^1 Sco. The data for Fe II λ2367 represent the first known detection of this very weak line (the vertical scale for this plot is expanded compared to the other profiles).

sitions and establish the methodologies with which the f-values for the other transitions are derived.

Our analysis is based primarily on use of the apparent optical depth method (see Savage & Sembach 1991), which allows us to take full advantage of the information available in the velocity-dependent profile structure. However, for consistency checks, we also utilize other independent techniques such as the curve of growth and line profile fitting where appropriate. In the case of the former, we generally restrict the use of the curve of growth to situations where the optical depth, τ, of the *strongest* line is less than 2 (Jenkins 1987). In the case of the latter, we adopt the profile fitting methodology and software discussed by Spitzer & Fitzpatrick (1993).

The apparent optical depth method is based upon expressing the observed line profiles in the form of apparent optical depth profiles versus velocity (Savage & Sembach 1991), which are defined as

$$\tau_a(v) = \ln [I_c(v)/I(v)] , \quad (1)$$

where $I(v)$ and $I_c(v)$ are the observed line and fitted continuum intensity at velocity v, respectively. From equation (1), the velocity-dependent apparent column density per unit velocity, $N_a(v)$, in units of cm^{-2} $(km\ s^{-1})^{-1}$, takes the form

$$N_a(v) = [\tau_a(v)/f\lambda_0]m_e c/\pi e^2 = [\tau_a(v)/f\lambda_0]3.768 \times 10^{14} , \quad (2)$$

where f is the line oscillator strength and λ_0 is the line rest wavelength (in units of angstroms). In the limit where the line profile is completely resolved, equation (2) expresses the true column density distribution $[N(v) = N_a(v)]$, and direct integration of $N(v)$ over velocity always yields the correct total column density. However, at the finite resolutions employed here, the possible presence of narrow, unresolved components in the data can give rise to *unresolved saturated structure*, which can seriously distort the apparent column density profiles and lead to an underestimate of total integrated apparent column density, $\int N_a(v)dv$, over the affected velocity range [for convenience, we define $N_a = \int N_a(v)dv$].

The possible presence of unresolved saturated structure can be explored by comparing two or more $N_a(v)$ profiles of the

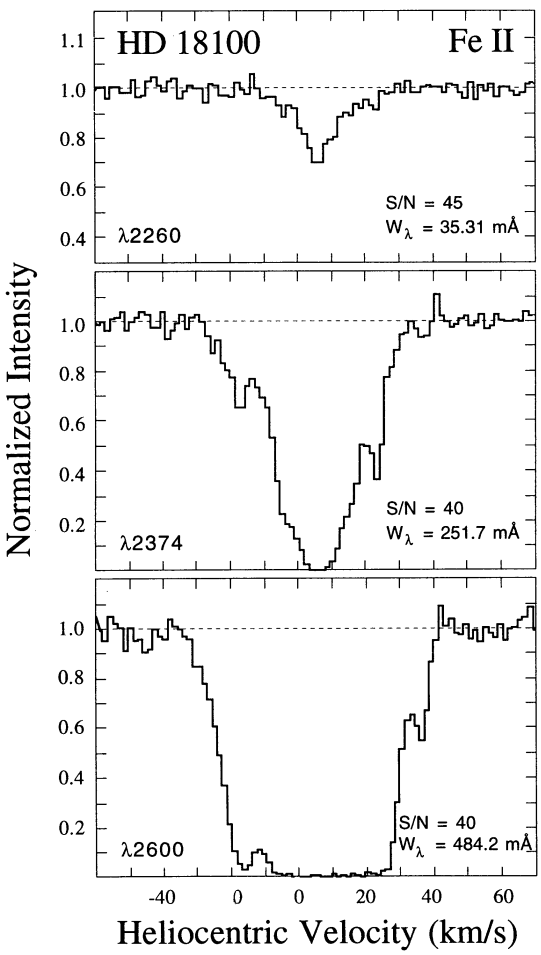

FIG. 2.—Same as Fig. 1, except for data in the sight line to HD 18100. This sight line shows a much broader and shallower component structure in comparison to the β^1 Sco profiles, which sharply cut off at the higher velocities.

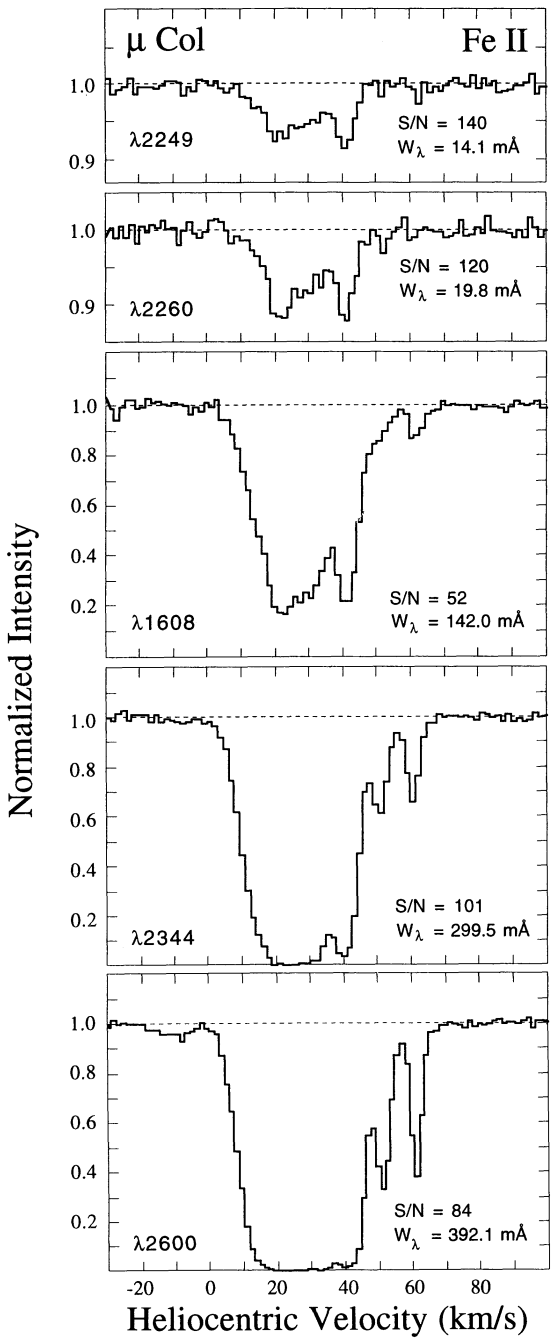

FIG. 3.—Same as Fig. 1, except for data in the sight line to μ Col. The data for Fe II λ1608 were obtained with the echelle A grating (3.5 km s^{-1} resolution). Like HD 18100, this sight line is dominated by gas showing a much broader and shallower component structure in comparison to the β^1 Sco profiles.

same species whose $f\lambda$ values are reasonably different (e.g., factor ≥ 2). When no significant unresolved saturated structure is present, the $N_a(v)$ profiles match each other at all values of v (see Fig. 3 in Cardelli, Sembach, & Savage 1995) and $N_a^{\text{line 1}} = N_a^{\text{line 2}} = N_{\text{true}}$. However, when unresolved saturated structure is present, the two profiles will diverge from each other over the saturated region (see Savage & Sembach 1991), with the stronger line exhibiting lower values of $N_a(v)$ *over the affected region*. In this case, the stronger line, and possibly also the weaker line, underestimates $N_a(v)$ (and hence the N_a). In general, the point at which unresolved saturated structure becomes a problem (i.e., some particular value of τ_a) will depend upon the width of the narrow components in relation to the spectral resolution and their fractional contribution to the total column density.

For our analysis of f-values, it is important to note the following. For data obtained at GHRS echelle resolutions, the deviations in $N_a(v)$ profiles due to unresolved saturated structure (if present) typically affect the stronger components (largest values of τ_a) much more than the weaker ones. Consequently, comparisons between log $N_a(v)$ profiles containing at least some unresolved saturated structure will exhibit these deviations in the form of a change in the relative profile shapes. On the other hand, errors in the relative f-values between any pair of lines will always appear only as a zero-point shift between log $N_a(v)$ profiles. It is therefore relatively straightforward to discriminate between the two effects.

In practice, it is possible to correct N_a for the presence of unresolved saturated structure, provided that the degree of unresolved saturation is not too large. For example, in the case of doublets (i.e., a pair of lines for which $\Delta \log f\lambda \simeq 0.3$), Savage & Sembach (1991) have shown that in most applications in which the difference in N_a between the lines is of the order of 0.1 dex or less ($\leq 25\%$), the correct total column density can be found by adding this difference to the N_a of the weaker line. In general, similar "correction" schemes can also be derived for

TABLE 2

MEASURED Fe II EQIVALENT WIDTHS AND ERRORS[a]

λ_0 (Å)[b]	Transition	β^1 Sco	HD 18100	μ Col
1142.3656....	$4s\,^6D_{9/2}$–$y\,^6F^o_{7/2}$	13.8 (0.8)[c]	...	...
1608.4511....	$y\,^6P^o_{7/2}$	...	...	142.1 (2.3)
1611.2005....	$y\,^4F^o_{7/2}$	12.8 (1.1)[c]	...	4.16 (1.20)
2249.8768....	$z\,^4D^o_{7/2}$	34.8 (0.8)	...	14.1 (1.0)
2260.7805....	$z\,^4F^o_{9/2}$	...	44.2 (4.0)	19.8 (1.4)
2344.214.....	$z\,^6P^o_{7/2}$	...	...	299.5 (2.8)
2367.5905....	$z\,^6F^o_{7/2}$	1.97 (0.33)	...	...
2374.4612....	$z\,^6F^o_{9/2}$	168.4 (1.7)	251.7 (2.5)	185.8 (2.4)
2382.765.....	$z\,^6F^o_{11/2}$	...	...	374.3 (3.7)
2586.6500....	$z\,^6D^o_{7/2}$	...	...	294.6 (3.0)
2600.1729....	$z\,^6D^o_{9/2}$	277.3 (2.8)	484.2 (4.8)	392.1 (3.9)

[a] Total equivalent widths, W_λ, in mÅ along with 1 σ errors in parentheses. All the data were obtained with the high resolution echelle gratings (R = 90,000) unless otherwise noted. The equivalent widths are for the complete multi-component absorption.

[b] Vacuum rest wavelengths (from Morton 1991).

[c] Data obtained with the medium resolution grating G160M (R = 20,000).

TABLE 3

Fe II BASELINE ATOMIC DATA[a]

λ_0 (Å)	Transition	f-value[b]
2249.8768.....	$4s\,^6D_{9/2}$–$z\,^4D^o_{7/2}$	0.00182 (14)
2260.7805.....	$z\,^4F^o_{9/2}$	0.00244 (19)

[a] Data used to establish the absolute scale from which the f-values for the other transitions are derived.

[b] These f-values are from Bergeson, Mullman, & Lawler (1994). The number in parenthesis beside each value is the uncertainty in the last digits. These experimental f-values were derived by combining accurate measures of branching fractions with accurate experimental lifetimes.

cases where $\Delta \log f\lambda$ exceeds 0.3 (see Savage et al. 1992 and below).

In the case of $\lambda 2249$ observed toward β^1 Sco, a direct integration of the line profile shown in Figure 1 yields $\log N_a = 14.74 \pm 0.02$. However, we suspect that some unresolved saturated structure might be present in the core of the line. High-resolution (0.5 km s^{-1}) optical spectra of Na I show four components with line widths (Δv = full width at half-maximum) ranging between 1 and 2 km s^{-1} within the main component observed at $v_{\rm helio} = -10$ km s^{-1} (Welty, Hobbs, & Kulkarni 1994). Unfortunately, we have no other weaker Fe II lines with reliable f-values from which to directly assess the presence of, or correction to, possible unresolved saturated structure. We resolve this problem through the analysis of transitions of Cr II, an element that is observed to behave similarly to Fe II in terms of component structure and the degree to which it is depleted onto dust grains (Savage et al. 1992; Cardelli et al. 1995). The observations of β^1 Sco included echelle B data for the Cr II triplet at $\lambda\lambda 2056$ ($W_\lambda = 29.2 \pm 1.6$ mÅ), 2062 ($W_\lambda = 23.2 \pm 0.9$ mÅ), and 2066 ($W_\lambda = 16.9 \pm 0.9$ mÅ) with $\log f\lambda = 2.335$, 2.206, and 2.027 (Bergeson & Lawler 1993b), respectively. For the weakest Cr II line we find $\log N_a = 12.99 \pm 0.02$, while for the strongest line, $\log N_a = 12.96 \pm 0.02$. Since these two lines correspond to $\Delta \log f\lambda \simeq 0.3$, the correction procedure of Savage & Sembach (1991) can be applied and suggests $\log N$(Cr II) $= 13.02 \pm 0.03$. A curve-of-growth fit to all three lines ($\tau \simeq 1$ for the strongest line) produces essentially identical results ($\log N$(Cr II) $= 13.01 \pm 0.04$ and $b = 3.3$ km s^{-1}, where b is the velocity spread parameter and is related to the line width by $\Delta v = 1.665b$). Because the equivalent width of $\lambda 2056$, the strongest of the Cr II lines, is nearly the same as that of Fe II $\lambda 2249$ (Table 2), it is reasonable to assume that the impact of unresolved saturated structure is also similar. This leads to a correction to N_a for $\lambda 2249$ that is approximately equal to $\log N$(Cr II) $- \log N_a^{\lambda 2056} \simeq 0.06 \pm 0.02$, giving $\log N$(Fe II) $= 14.80 \pm 0.04$ (the error includes both the uncertainty in the correction and in $f_{\lambda 2249}$).

As a check on our $N_a(v)$ analysis, we also derived N(Fe II) by forcing $\lambda 2249$ to fit the curve of growth defined by the Cr II lines. Again, this is reasonable since we can expect that the absorption from Cr II and Fe II trace each other quite well. Adopting $b \simeq 3.3$ km s^{-1} from the Cr II fit, we find $\log N$(Fe II) $= 14.79$. We also derived N(Fe II) through profile fitting. Using Fe II $\lambda 2374$ as an additional guide to the component structure, we fitted $\lambda 2249$ with four components located at $v_{\rm helio} \simeq -10$, -16, -24, and -30 km s^{-1} (see Fig. 1). The fit yields $\log N$(Fe II) $= 14.81$ with about 85% of the total column density residing in the main component at $v_{\rm helio} = -10$ km s^{-1}. We find the same result if we employ the more detailed component structure indicated by the high-resolution Na I study of Welty et al. (1994).

For Fe II $\lambda 2260$ observed toward HD 18100, we followed the same procedures as above. However, based on a similar comparison to the available Cr II lines for this sight line, we find that no correction to $\log N_a$ is required even though $\tau_a \simeq 0.35$ at line center (the profiles observed toward β^1 Sco show evidence of unresolved saturation for $\tau_a \simeq 0.30$). A direct integration of $\lambda 2260$ yields $\log N$(Fe II) $= 14.64 \pm 0.05$ (this includes the uncertainty in $f_{\lambda 2260}$). The absence of unresolved saturated structure in this line is not surprising. Analyses of other "similar" sight lines probing relatively warm, low-density disk and halo gas (HD 167756, Cardelli et al. 1995; HD 93521, Spitzer & Fitzpatrick 1993; μ Col, Sofia et al. 1993) indicate a much smaller contribution from cold, narrow components compared to denser sight lines like β^1 Sco. Consequently, the effects of unresolved saturated structure generally begin to appear only at substantially larger apparent optical depths (see below).

For μ Col, both Fe II $\lambda\lambda 2249$ and 2260 were observed, and direct integration of these lines produces results that differ by only 0.01 dex from which we find $\log \langle N$(Fe II)$\rangle = 14.26 \pm 0.03$. As with HD 18100, the warm, low-density nature of the gas in the μ Col sight line allows direct "correction-free" integration to rather modest optical depths, well in excess of the τ_a values for these two lines (see Sofia et al. 1993 and below). However, as a check, we also compute N(Fe II) by assuming that the data are on the linear portion of the curve of growth, where $N = 1.13 \times 10^{20} W_\lambda / f\lambda_0^2$. For the pair of lines we find $\log \langle N$(Fe II)$\rangle = 14.25 \pm 0.03$. The (minor) difference from the value derived from the N_a is insignificant, and so we conclude that there is in fact no line saturation.

3.2. *Weak* Fe II *Lines: f-values for* $\lambda\lambda 1142$, *1611, and 2367*

Data for Fe II $\lambda\lambda 1142$, 1611, and 2367 were obtained for β^1 Sco, and so the following discussion pertains to this sight line only. The f-values for these three transitions, which are all weaker than $\lambda 2249$ (i.e., smaller in W_λ/λ), are explored in the following way. First, we apply elements of the apparent optical depth method discussed in the previous section to determine the appropriate corrections for unresolved saturated structure to the computed N_a, initially derived using the f-values listed by M91, f_m. Second, from equation (2) and noting that corrections to the N_a are multiplicative in nature, the correct f-value, $f_{\rm new}$, is found from a comparison between N(Fe II)$_{\lambda 2249}$ obtained from the analysis of $\lambda 2249$ discussed above and the corrected N_a, N(Fe II)$_c$, through

$$f_{\rm new} = f_m [N(\text{Fe II})_c / N(\text{Fe II})_{\lambda 2249}] \, . \qquad (3)$$

The computed uncertainty associated with $f_{\rm new}$ follows from a propagation of the errors in N(Fe II)$_{\lambda 2249}$ and N(Fe II)$_c$ that includes the uncertainty in the N_a correction. However, note that since $N(\text{Fe II})_c \propto f_m^{-1}$, the computed uncertainty is not dependent on f_m or $\sigma(f_m)$ but rather on $f_m N(\text{Fe II})_c = (3.768 \times 10^{14}/\lambda_0)[\int \tau_a(v) dv]$ (from eq. [2]).

For Fe II $\lambda 2367$ ($W_\lambda = 1.97 \pm 0.33$ mÅ), the line is so weak ($\tau_a^{\rm max} = 0.04$) that no correction to N_a is required. This can be seen by noting that the N_a ($= 2.48 \times 10^{14}$ cm^{-2} using $f_m = 1.60 \times 10^{-4}$) is identical to the column density derived from the assumption that the line resides on the linear portion of the curve of growth. From equation (3), we find $f_{\rm new} = 6.28(\pm 1.13) \times 10^{-5}$, a decrease in f_m by a factor 2.5.

For Fe II $\lambda\lambda 1142$ ($W_\lambda = 13.83 \pm 0.75$ mÅ) and 1611 ($W_\lambda = 12.80 \pm 1.1$ mÅ), the lines are strong enough that some unresolved saturated structure is expected, especially considering the fact that these data were obtained with the medium-resolution G160M grating. In the absence of weaker Fe II transitions at this resolution (or for that matter, transitions of other species with similar characteristics) with which to explore the presence of unresolved saturated structure as we did for Fe II $\lambda 2249$, we took the high-resolution echelle B observations of both Fe II $\lambda 2249$ and the Cr II triplet and smeared them to the equivalent resolution of the G160M grating. Since we were able to derive absolute column densities for Fe II and Cr II from the echelle B data, we can construct an empirical relationship between $\Delta \log N = \log N_{\rm total} - \log N_a^i$ and a measure of the relative line strength like $\log W_\lambda/\lambda$ (we could have also used a

line strength parameter like τ_a at line center), where i refers to a particular transition. The Fe II and Cr II lines used to construct this empirical relationship suit our needs quite well since their relative line strengths bracket those of $\lambda\lambda$1142 and 1611 (log W_λ/λ for λ1611 is about the same as Cr II λ2066). A least-squares fit to this empirical relationship gives $\Delta \log N = 0.326$ (log W_λ/λ) + 1.695 with a correlation coefficient of $r^2 = 0.98$. The data along with the fit are shown in Figure 4.

Using the above empirical fit, we derive corrected column densities of $N(\text{Fe II})_c = 3.12 \times 10^{14}$ cm^{-2} (using $f_m = 5.00 \times 10^{-3}$) and 2.89×10^{15} cm^{-2} (using $f_m = 2.22 \times 10^{-4}$) for $\lambda\lambda$1142 and 1611, respectively. Applying equation (3), we find $f_{\text{new}} = 2.47(\pm 0.32) \times 10^{-3}$ for λ1142 (a factor 2 smaller than f_m) and $f_{\text{new}} = 1.02(\pm 0.14) \times 10^{-3}$ for λ1611 (a factor 4.6 larger than f_m).

As an independent check of these new f-values, we fitted the weak line data with a theoretical curve of growth. Figure 5 shows the curve of growth for all the data, including λ2249. In Figure 5*a*, the data are plotted using the f-values (f_m) from M91 for all the lines. Problems with these f-values are readily apparent. Figure 5*b* shows the curve of growth using the f-values (f_{new}) derived above and $f_{\lambda 2249}$ from Bergeson et al. (1994). Also shown is the fit ($\chi^2 = 0.03$) using the theoretical curve of growth along with the derived fit parameters and the corresponding line optical depths. Given that $\tau < 2$ for the strongest line, use of the theoretical curve of growth should be valid (Jenkins 1987). In addition to the high quality of the fit and the excellent agreement between log N_{best} and log N(Fe II) derived from our analysis of λ2249, the derived value of b agrees quite well with the value obtained from the independent fit to the Cr II triplet, as we expect it should.

3.3. *Strong* Fe II *Lines: f-values for* $\lambda\lambda$*1608, 2344, 2374, 2382, 2586, and 2600*

Data for Fe II $\lambda\lambda$2374 and 2600 were obtained for all three sight lines, while for Fe II $\lambda\lambda$1608, 2344, 2382, and 2586, we only have data for the μ Col sight line. For β^1 Sco, the analysis is based on a comparison to λ2249. For HD 18100, we use λ2260 (using $f_{\lambda 2260}$ from Bergeson et al. 1994). For μ Col, both $\lambda\lambda$2249 and 2260 are used. Where possible, the results for lines in common between sight lines are combined together in determining f_{new}. We also employ independent checks of the derived f-values (e.g., curve of growth and profile fitting where possible) to help ensure that the results are self-consistent *within and between* the different sight lines.

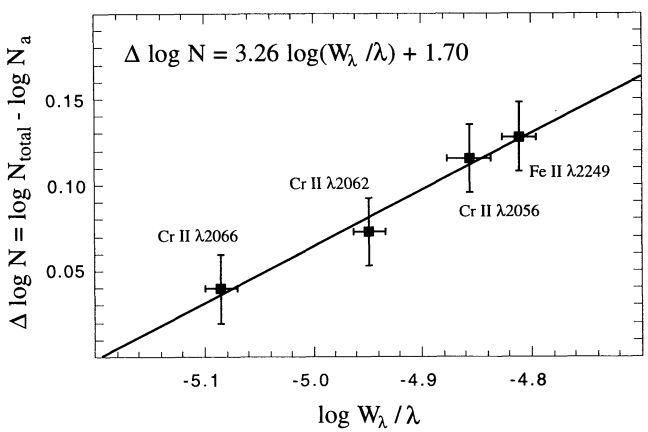

FIG. 4.—The differences between the logarithm of the *adopted* column densities for Cr II and Fe II (derived from the echelle data) and the logarithm of the direct integration of these same data smeared to the resolution of the medium dispersion grating G160M plotted against log W_λ/λ. The linear least-squares fit to these data along with the fit equation are also shown. This fit is used to determine the correction to N_a for the Fe II lines observed with the G160M grating.

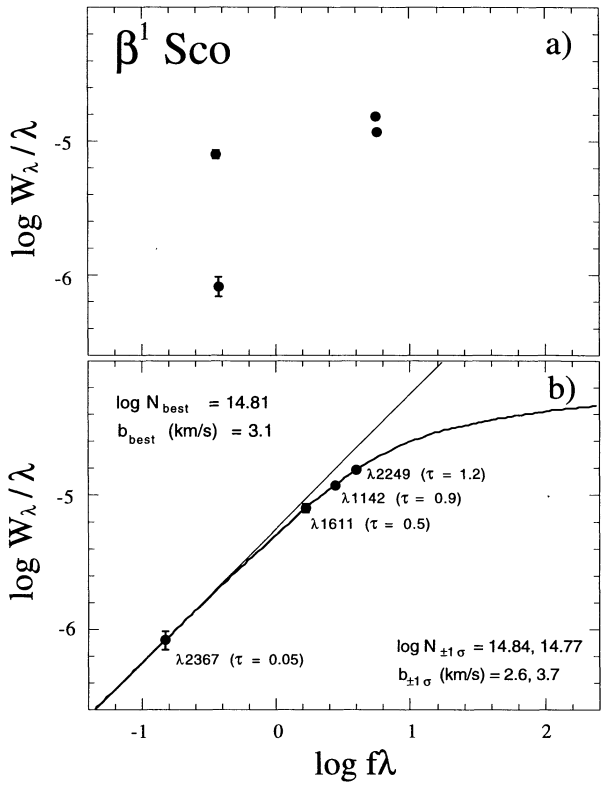

FIG. 5.—Empirical curve of growth for the weak Fe II lines observed toward β^1 Sco plotted using (*a*) the f-values listed in Morton (1991) and (*b*) the f-values derived in this paper. Also shown in (*b*) is the fit ($\chi^2 \simeq 0.03$) using a theoretical curve of growth and the resulting fit values. The derived log N_{best} is in excellent agreement with the value derived from the integrated apparent column density profile, $N_a(v)$, of λ2249 corrected for the effects of unresolved saturated structure (see text). The value of b obtained from this fit is also in excellent agreement with the one found for the observed Cr II triplet, a species expected to behave similarly to Fe II.

For β^1 Sco and HD 18100, the absorption for λ2374 and especially λ2600 in the deepest portions of the profiles (see Figs. 1 and 2) is so strong ($\tau_a \gg 4$) that none of the analysis techniques discussed here are capable of producing sufficiently accurate results in these strongly absorbing regions. With the exception of $\lambda\lambda$1608 and 2374, the same also applies to the lines observed toward μ Col. Consequently, we cannot rely on simple comparisons involving computing total Fe II column densities, and so we analyze the data by concentrating on an analysis of the $N_a(v)$ profiles for the weaker absorption components. Therefore, f_{new} is determined for each line i from a comparison of the computed $N_a(v)$ profiles over velocities *where there is no unresolved saturated structure* by replacing $N(\text{Fe II})_c/N(\text{Fe II})_{\lambda 2249}$ in equation (3) with $\langle N_a(v)_i/N_a(v)_{\lambda\lambda 2249,2260}\rangle$.

For Fe II λ2249 observed toward β^1 Sco, the *strongest* absorption for $v_{\text{helio}} < -15$ km s^{-1} corresponds to $\tau_a \simeq 0.1$. For λ2374, the absorption over this same velocity range varies in strength from a minimum detection limit (i.e., a line depth of 2 σ relative to the continuum rms) of $\tau_a \simeq 0.01$ to a maximum

of $\tau_a \simeq 1.6$ at $v_{\rm helio} \simeq -24$ km s^{-1}. A direct comparison of the logarithm of the computed $N_a(v)$ profiles for these two lines shows that they have the same *shape* for $v_{\rm helio} < -15$ km s^{-1}, with the exception of a few points in the core of the λ2374 component at $v_{\rm helio} \simeq -24$ km s^{-1} that appear slightly weaker in $N_a(v)$ (see Fig. 6). This suggests the presence of some unresolved saturated structure, which is supported by the Na I data of Welty et al. (1994), which shows two components near $v_{\rm helio} \simeq -23$ km s^{-1} of nearly equal column density but with $\Delta v = 3.3$ and 0.9 km s^{-1}.

Given (1) the range of τ_a values covered by the λ2374 profile where it overlaps λ2249 for $v_{\rm helio} < -15$ km s^{-1} ($0.3 \leq \tau_a \leq 1.4$), (2) the large difference in relative absorption strength for these two lines (a factor 16), *and* (3) the fact that we expect no unresolved saturated structure for the relatively weak absorption ($\tau_a^{\rm max} \leq 0.1$) from λ2249 over this velocity range, we conclude that little, if any, unresolved saturated structure is present in λ2374 as well for $v_{\rm helio} < -15$ km s^{-1}. The exceptions to this are the few points at $v_{\rm helio} \simeq -24$ km s^{-1} for λ2374.

Using Fe II λ2260 for HD 18100 and an average of $N_a(v)$ $\lambda\lambda$2249 and 2260 for μ Col, we performed the same analysis on λ2374 as above. For the HD 18100 data over $v_{\rm helio} < +5$ km s^{-1} and the μ Col data over $v_{\rm helio} < +36$ km s^{-1} (see Figs. 2 and 3), comparison of the $N_a(v)$ profiles shows no noticeable deviations in the profile shape with $v_{\rm helio}$ for either sight line, again indicating no unresolved saturated structure. However, this is not unexpected. As discussed above, sight lines like HD 18100 and μ Col probing warm and relatively low density gas tend to show a significantly smaller contribution from narrow components. Consequently, direct "correction-free" integration to larger optical depths is possible in comparison to sight lines like β^1 Sco. The significance of this can be appreciated by noting that $\tau_a(v) \simeq 4$ for the HD 18100 data of λ2374 at $v_{\rm helio} \simeq +4$ km s^{-1}. In comparison, the data for β^1 Sco show the effects of unresolved saturated structure for $\tau_a(v) \geq 0.3$.

Combining together the results for these three sight lines using $f_m = 2.82 \times 10^{-2}$ for λ2374 (M91) and the f-values from Table 3 for $\lambda\lambda$2249 and 2260, we find $\langle N_a(v)_{\lambda 2374} / N_a(v)_{\lambda 2249,2260} \rangle = 1.16 \pm 0.07$. Application of the modified equation (3) then gives $f_{\rm new} = 3.26(\pm 0.23) \times 10^{-2}$. The quoted uncertainties include the uncertainty in $f_{\lambda 2249}$ and $f_{\lambda 2260}$). Using $f_{\rm new}$, we plot the log $N_a(v)$ profiles for λ2374 for β^1 Sco and HD 18100 in Figures 6 and 7 along with the log $N_a(v)$ profiles for $\lambda\lambda$2249 and 2260. For the λ2374 data for β^1 Sco, the points at $v_{\rm helio} \simeq -24$ km s^{-1} exhibiting unresolved saturated structure have been included in the plot but have been omitted from the analysis. The bottom panels in both figures show the logarithm of the $N_a(v)$ ratios. Both are consistent with a ratio of about unity (the same result is found for the μ Col data). Considering the diversity of these three sight lines and the range of

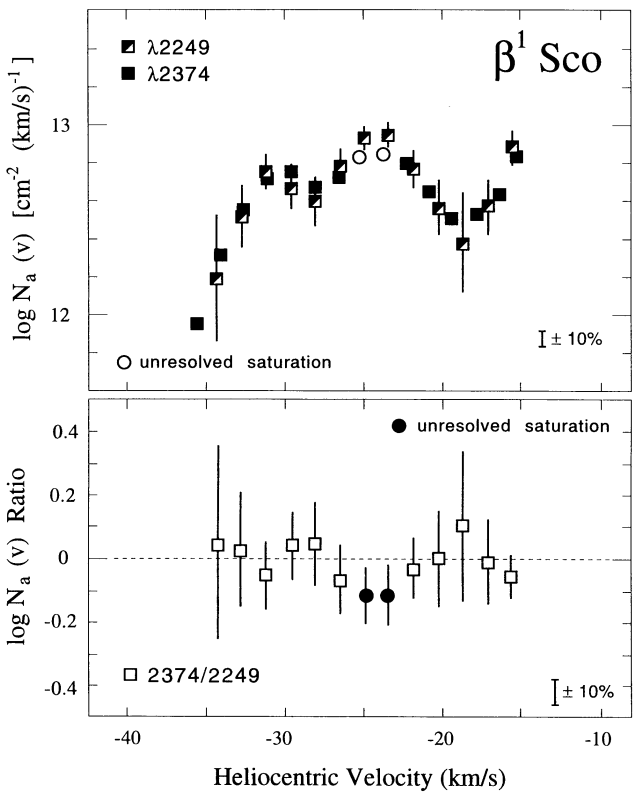

FIG. 6.—A portion of the logarithm of the $N_a(v)$ profiles for Fe II $\lambda\lambda$2249 and 2374 observed toward β^1 Sco derived using the f-value of Bergeson et al. (1994) for λ2249 and the one for λ2374 derived here (*top*). The excellent agreement between these $N_a(v)$ profiles, which cover a large variation in τ_a (see Fig. 1), indicates that no unresolved saturation is present over this velocity range. The exceptions to this are the few points flagged as containing unresolved saturated structure. These points have not been included in the derivation of the new f-value. The bottom panel shows the logarithm of the ratio between the $N_a(v)$ profiles.

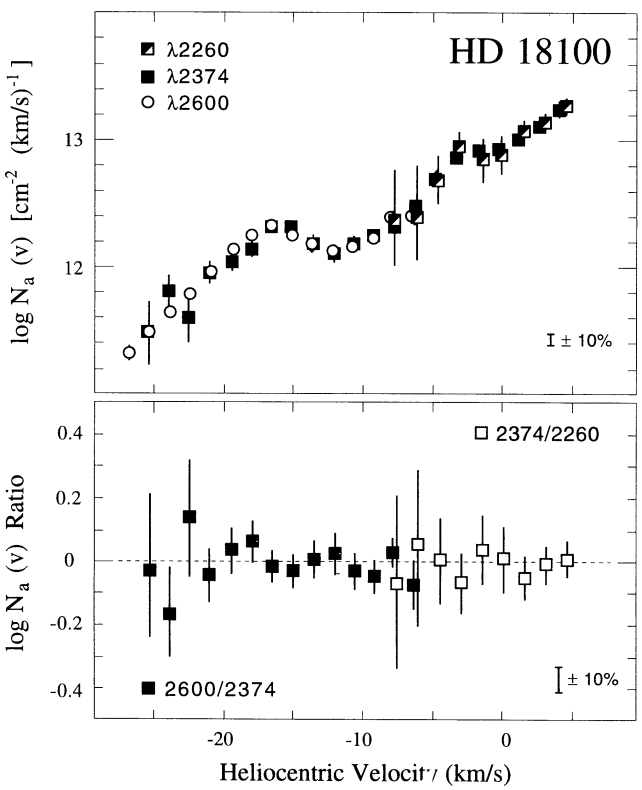

FIG. 7.—A portion of the logarithm of the $N_a(v)$ profiles for Fe II $\lambda\lambda$2260, 2374, and 2600 observed toward HD 18100 derived using the f-value of Bergeson et al. (1994) for λ2260 and the f-values derived here for $\lambda\lambda$2374 and 2600 (*top*). The excellent agreement between these $N_a(v)$ profiles, which cover a large variation in τ_a (see Fig. 2), indicates that no unresolved saturation is present over this velocity range. The bottom panel shows the logarithm of the $N_a(v)$ ratio of $\lambda\lambda$2374/2260 and $\lambda\lambda$2600/2374.

τ_a values sampled, the consistency of these ratios discounts any possible (systematic) influence of unresolved saturated structure in the determination of f_{new}.

A comparison between the $N_a(v)$ of λ2374 using the new f-value and λ2600 using $f_m = 2.44 \times 10^{-1}$ over $v_{helio} < -6$ km s^{-1} for HD 18100 and $v_{helio} < 12$ km s^{-1} for μ Col shows no unresolved saturated structure over these velocity regions (the relative line strengths differ by about a factor 10). This includes values of τ_a as large as 4 for the λ2600 profiles (see Figs. 2 and 3). However, this comparison does indicate that $f_{\lambda 2600}$ needs to be decreased by about 5% to a value of $f_{new} = 2.13(\pm 0.18) \times 10^{-1}$. For the HD 18100 data, $N_a(v)$ for λ2600 using this new f-value is shown in Figure 7 in comparison to λ2374. The bottom panel shows log $[N_a(v)_{\lambda 2600}/N_a(v)_{\lambda 2374}]$ for which we find $\langle N_a(v)_{\lambda 2600}/N_a(v)_{\lambda 2374} \rangle = 1.01$.

The analysis of the remaining lines, Fe II $\lambda\lambda$1608, 2344, 2382, and 2586, observed toward μ Col follows from the discussion above. Where possible, direct comparisons were made with $\langle N_a(v)_{\lambda\lambda 2249, 2260} \rangle$. However, for the strongest lines we also used the $N_a(v)$ of λ2374 computed with the new f-value. Results analogous to those shown in Figures 6 and 7 are shown in Figure 8 for $\lambda\lambda$1608 and 2344. We find excellent agreement between the $N_a(v)$ profiles for these two lines using the f-values given by M91 and $\langle N_a(v)_{\lambda\lambda 2249, 2260} \rangle$. Our analysis of λ2382 also shows good agreement using the M91 f-value. However, analysis of the data for λ2586 indicates that the f-value needs to be increased by about 6% to a value of $f_{new} = 6.84(\pm 0.55) \times 10^{-2}$.

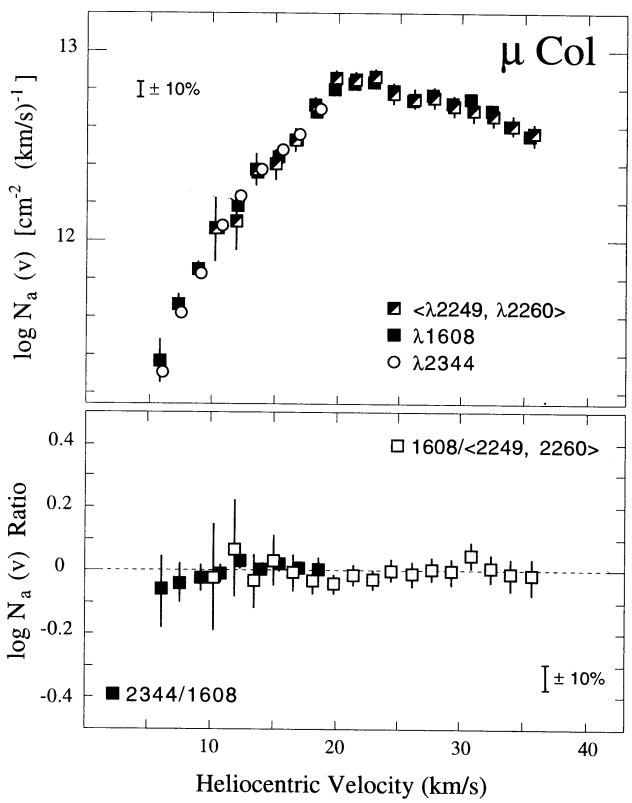

FIG. 8.—A portion of the logarithm of the $N_a(v)$ profiles for Fe II $\lambda\lambda$1608 and 2344 and an average of the $N_a(v)$ profiles for $\lambda\lambda$2249 and 2260 observed toward μ Col derived using the f-value of Bergeson et al. (1994) for $\lambda\lambda$2249 and 2260 and the f-values for $\lambda\lambda$1608 and 2344 taken from Morton (1991) (*top*). The excellent agreement between these $N_a(v)$ profiles, which cover a large variation in τ_a (see Fig. 3), indicates that no unresolved saturation is present over this velocity range. The bottom panel shows the logarithm of the $N_a(v)$ ratio of $\lambda\lambda$1608/$\langle$2249, 2260$\rangle$ and $\lambda\lambda$2344/1608.

As an independent check of our results, we took the μ Col data from Table 2 for all the transitions discussed in this section and fitted them with a theoretical curve of growth. Since the stronger lines have τ values derived from the curve-of-growth fit ranging between 1.6 (λ2374) and 14 (λ2382), this would seem to strongly violate the convention that, in general, the strongest line should have $\tau < 2$ (Jenkins 1987). However, the μ Col sight line is an example of an exception to this in that the bulk of the column density corresponds to very broad component structure centered around $v_{helio} \simeq 25$ km s^{-1} (see Fig. 3) that is being resolved by the GHRS echelle grating. For example, from a direct integration of the $N_a(v)$ profiles for $\lambda\lambda$2374 and 1608, we obtain log $N_a = 14.26 \pm 0.01$ and 14.25 ± 0.02, respectively. Even for λ2344, for which the curve of growth indicates $\tau = 5$, we find log $N_a = 14.24 \pm 0.04$.

A curve-of-growth fit to all the lines, including $\lambda\lambda$2249 and 2260, yields log N(Fe II) = 14.27 ± 0.01 and $b = 13.23 \pm 0.12$ km s^{-1} with $\chi^2 = 1.1$. Since weak lines dominate the determination of log N, while the strong lines dominate the determination of b, we also fitted the data by excluding $\lambda\lambda$2249 and 2260. From this we find log N(Fe II) = 14.27 ± 0.01 and $b = 13.27 \pm 0.13$ km s^{-1} with $\chi^2 = 0.8$. The excellent agreement between these results and those derived from a direct $N_a(v)$ analysis of $\lambda\lambda$2249 and 2260 [log N(Fe II) = 14.26 ± 0.03] strongly supports our use of the curve of growth for this sight line and our contention that we are effectively resolving the dominant component structure. More importantly, the small χ^2 values from these fits provide confirmation of the new f-values we derived from our $N_a(v)$ analysis. Consider for comparison the results obtained if we do the same curve of growth fit to all the lines but use the f-values given in M91 for all the lines (except Fe II $\lambda\lambda$2249 and 2260 for which we use the experimental values from Table 3). From this fit we find log N(Fe II) = 14.32 ± 0.01 and $b = 12.85 \pm 0.10$ km s^{-1} and more importantly, $\chi^2 = 25$.

4. DISCUSSION

4.1. *New* Fe II *f-values: Summary of Results*

The results of our Fe II f-value analyses are summarized in Table 4 along with the f-values listed by M91 and the references from which these values were obtained. Independent checks (e.g., curve of growth and profile fitting where possible) of the derived f-values among the three sight lines show these results to be self-consistent. The 1 σ errors listed for the literature f-values derive from the 3 σ values computed by M91. The 1 σ errors listed for the f-values derived here come from the statistical analysis of the data and include the quoted measurement uncertainties (8%) for $f_{\lambda 2249}$ and $f_{\lambda 2249}$ from Bergeson et al. (1994). In this regard, these are *absolute uncertainties* for each line and are *applicable when only a single line is used.* Since a portion of these errors is derived from the uncertainties in $f_{\lambda 2249}$ and $f_{\lambda 2249}$, the quoted errors are coupled when more than one line is used, and the applicable error will subsequently be smaller. More specifically, the *relative* uncertainties in the f-values are about a factor 2 smaller than those listed in Table 4.

For the strongest lines (i.e., Fe II $\lambda\lambda$2344, 2382, and 2600), the analysis here shows that to within the mutual errors, the f-values listed by M91 are quite reasonable. The f-values we

TABLE 4

Fe II Resonance Line Transition *f*-Values[a]

λ_0 (Å)	Transition	*f*-Values (This work)[a]	*f*-values (Other)[b]	Reference
1142.3656.....	$4s\,^6D_{9/2}$–$y\,^6F^o_{7/2}$	0.00247 (32)	0.00500 (175)	1, 2
1608.4511.....	$y\,^6P^o_{7/2}$	0.0619 (62)	0.0619 (186)	2, 3
1611.2005.....	$y\,^4F^o_{7/2}$	0.00102 (14)	0.000222	1
2249.8768.....	$z\,^4D^o_{7/2}$	0.00182 (14)[c]	0.00182 (14)[c]	4
2260.7805.....	$z\,^4F^o_{9/2}$	0.00244 (19)[c]	0.00244 (19)[c]	4
2344.214	$z\,^6P^o_{7/2}$	0.110 (8)	0.110 (8)	3, 5, 6
2367.5905.....	$z\,^6F^o_{7/2}$	0.0000628 (113)	0.000160 (11)	3, 5, 6
2374.4612.....	$z\,^6F^o_{9/2}$	0.0326 (23)	0.0282 (20)	3, 5, 6
2382.765	$z\,^6F^o_{11/2}$	0.300 (21)	0.300 (21)	3, 5, 6
2586.6500.....	$z\,^6D^o_{7/2}$	0.0684 (55)	0.0646 (45)	5, 6
2600.1729.....	$z\,^6D^o_{9/2}$	0.213 (18)	0.224 (16)	5, 6

[a] The *f*-values derived in this paper. The number in parenthesis beside each value is the 1 σ uncertainty in the last digits. Our absolute *f*-values are referenced to the laboratory measures of Bergeson, Mullman, & Lawler 1994 for the Fe II $\lambda\lambda$2249, 2260 lines.

[b] These *f*-values were obtained from the listing of Morton 1991 except where noted. The original references from which he obtained these values are given in the fifth column. The listed 1 σ uncertainties in parenthesis derive from the 3 σ values computed by Morton 1991.

[c] These *f*-values are from the laboratory work of Bergeson et al. 1994.

References.—(1) Kurucz 1989, theory (see Morton 1991); (2) Shull, van Steenberg, & Seab 1983, ISM absorption (see also Lugger et al. 1982); (3) Nussbaumer, Pettini, & Storey 1981, theory, (4) Bergeson et al. 1994, measured branching ratios and radiative lifetimes; (5) Fuhr, Martin, & Wiese 1988, compilation; (6) Biemont et al. 1991, laser excitation lifetimes.

derive for the moderate-strength lines (i.e., $\lambda\lambda$1608, 2374, and 2586) also compare favorably with M91, except for λ2374. However, for the weak lines $\lambda\lambda$1142, 1611, and 2367 we find differences from the M91 values ranging between a factor 2 and 5. The *f*-values for these transitions listed by M91 were taken from the literature sources given in Table 4 and were derived from both theory and empirical (ISM) analysis. In the case of the theoretical calculations, large errors can occur given the complex nature of the atomic structure of Fe II. The large number of transitions observed within many Fe II multiplets coupled with the relatively close spacing in energy *between* individual multiplets underscores the fact that serious mixing of different energy states occurs, which leads to serious overlap between the individual multiplet wave functions. If this interaction is not correctly accounted for, large errors in the atomic constants can result.

In the case of the empirical ISM *f*-value work (e.g., Lugger et al. 1982; Shull, van Steenberg, & Seab 1983), a major problem arises because the analyses relied principally on relatively strong lines to establish the curve-of-growth fit from which the weaker line *f*-values were derived. The majority of the strong lines used in these studies, which included the lines analyzed here, have typical values of τ well in excess of 2 for most of the sight lines studied. While these studies did include sight lines like μ Col, in which such curve-of-growth fits appear to be valid, the lower resolution *Copernicus* (13 km s^{-1}) and especially *IUE* (25 km s^{-1}) data sets that were used prevent a detailed assessment of the component structure and the possible (dominant) presence of narrow saturated components along with broader, more resolved structure. More times than not, the presence of multiple component structure will result in curve-of-growth fits based on such strong lines that (sometimes seriously) *underestimate* the total column density (Jenkins 1987), leading to systematic overestimates of weak line *f*-values. For example, the *f*-values for $\lambda\lambda$1142 and 2260 derived by Lugger et al. (1982) and Shull et al. (1983) are a factor 2 and 1.2 larger, respectively, than the ones given in Table 4. An extreme example of this effect can be seen for the gas observed toward β^1 Sco. Unlike μ Col, most of the column density in the β^1 Sco sight line occurs in very narrow, unresolved components near $v_{\rm helio} \simeq -10$ km s^{-1} (see Welty et al. 1994) together with weaker, broader components. Referring to Figure 1 for the λ2249 profile, most of the equivalent width (about 85%) resides in this main component. In comparison, the main component of the λ2374 profile has become strongly saturated. At the same time, the weaker negative velocity components, which have grown considerably in strength, have not yet become seriously saturated. In sharp contrast to λ2249, the main component for λ2374 contains only about 50% of the total equivalent width. Consequently, these two lines are no longer consistent with a fit to a *single* theoretical curve of growth because the applicable curves of growth for these two distinct absorbing complexes are *inherently different* (i.e., different log N and b). For example, if we were to place Fe II $\lambda\lambda$2374 and 2600 on the weak-line curve of growth for β^1 Sco in Figure 5*b*, they would reside about +0.3 dex above the fitted curve. Conversely, if we fit $\lambda\lambda$2374 and 2600 with a theoretical curve of growth, we find a b-value about a factor 2 larger and a column density about a factor 1.5 smaller than for the weak lines only. This problem can be generally reconciled by considering curve-of-growth fits for the individual absorbing regions but is *possible only with data of sufficient resolution* (i.e., at least 3–4 km s^{-1}).

4.2. *Scientific Requirements and Benefits*

In the analysis of ISM absorption, particularly in cases where atomic abundances are sought, observers should use fairly weak transitions so that corrections for effects like saturation can be minimized. This is especially true for sight lines through diffuse molecular clouds like β^1 Sco and ζ Oph (Savage et al. 1992) in which absorption from cold, narrow components is often strong. In these cases, reliable *f*-values for such transitions are of paramount importance. However, one should not conclude from this that strong lines are unimportant or unusable for abundance studies. For example, in sight lines like HD 18100 and μ Col as we have seen here, the lack of strong narrow components often means that even strong pro-

files like λ2374 can contain usable column density information down to very large absorption optical depths (provided the data are of sufficient resolution). In this context, strong lines are also useful in applications in which the total abundance in the absorbing column is low, such as can be the case in QSO absorption-line systems characterized by low N(H I), low metallicity, or both (e.g., see the recent Keck Telescope observations of Songaila et al. 1994 and Wolfe et al. 1994). In some cases, the weakest lines may not be detectable and so one *must* rely on the stronger transitions for deriving abundances. In order to link successfully the results of these various types of studies of Fe II abundances, it is imperative that accurate, self-consistent f-values are available for a large range of line strengths. The results presented here go a long way toward this goal by supplying accurate f-values for transitions having a total range in absorption strength ($f\lambda$) of nearly a factor 5000. For QSO absorption-line studies, the middle UV transitions (i.e., 2200 Å $< \lambda <$ 2600 Å) are particularly useful in that they are closely spaced in wavelength and accessible in the optical even in relatively low redshift systems (Meyer, Welty, & York 1989; Meyer & York 1992; Steidel et al. 1995).

Even when their cores are highly saturated, strong lines can also be very useful in that they are sensitive to very low column densities at velocities far from the saturated portion of the line. When coupled together with the results derived from absorption from weaker transitions, these data can be very useful for tracing accurate abundance variations over a large range of velocity and absorption strength. An example of this is shown in Figure 9, where we plot the composite log $N_a(v)$ Fe II profile for β^1 Sco. These data derive from using the new f-value data given in Table 4 and splicing together only the portions of the $N_a(v)$ for a given transition in which there is no unresolved saturated structure present. It is important to point out that we did not use the data for β^1 Sco in our analysis of the f-value of λ2600, principally because the $N_a(v)$ profile over the usable (unsaturated) portions is changing rapidly with velocity and small uncertainties in the velocity scale can lead to uncertainties in the derived f-value. However, Figure 9 shows that for $v_{\rm helio} < -33$ km s^{-1}, the data are consistent with our f-value assessment from the HD 18100 and μ Col data.

The composite $N_a(v)$ data for β^1 Sco are especially remarkable in that they allow us to trace variations in column density with velocity in this sight line over a range of a factor 10,000. With the availability of other analogous $N_a(v)$ profiles for species like Si, this type of information can be used to explore such things as variations in gas abundance ratios and the chemical characteristics of dust (e.g., Sofia, Cardelli, & Savage 1994) over a large range of interstellar gas conditions *in a single sight line.*

One other point on the composite $N_a(v)$ data for β^1 Sco data is important. For $v_{\rm helio} > -2$ km s^{-1}, the data for λ2600 appear to flare out rather smoothly. This behavior is a characteristic signature of the presence of damping wings (see measurements for ξ Per in Savage et al. 1991), which can also be very useful for deriving column densities, particularly when useful weak-line data are unavailable (see Cardelli et al. 1991 and Sofia et al. 1994). This damping wing arises from the main absorbing component located at $v_{\rm helio} \simeq -10$ km s^{-1}. The other damping wing is expected to extend from about -18 to -30 km s^{-1}. However, it is masked by absorption from the negative velocity gas. The gas column density associated with the components located at $v_{\rm helio} \simeq -24$ and -30 km s^{-1}, which represent only about 15% of the total N(Fe II), is insufficient to produce observable damping wings.

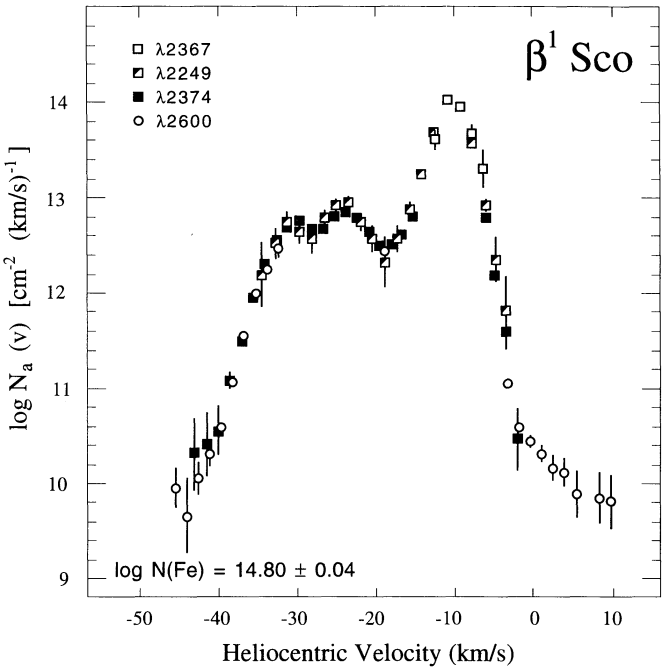

FIG. 9.—The logarithm of the composite Fe II $N_a(v)$ for the data observed toward β^1 Sco using the new f-values derived in this paper. Portions of the $N_a(v)$ profile in which there is unresolved saturated structure have not been plotted. The range of variation in $N_a(v)$ with velocity corresponds to a sensitivity of better than 1 part in 10,000 and allows us to trace variations in Fe II over a large dynamic range in this relatively nearby sight line. The apparent flaring in log $N_a(v)$ seen at $v_{\rm helio} > -2$ km s^{-1} corresponds to absorption in the damping wing produced by the strong component at $v_{\rm helio} \simeq -10$ km s^{-1} (see text).

We would like to acknowledge many useful discussions on this topic with S. Bergeson, S. Federman, J. Lawler, K. Sembach, and especially D. Morton. J. A. C. acknowledges support from NASA-LTSARP grant NAGW-2520. B. D. S. acknowledges support from NASA grant NAG 5-1852.

REFERENCES

Bergeson, S. D., & Lawler, J. E. 1993a, ApJ, 414, L137
———. 1993b, ApJ, 408, 382
Bergeson, S. D., Mullman, K. L., & Lawler, J. E. 1994, ApJ, 435, L157
Biemont, E., Baudoux, Kurucz, R. L., Ansbacher, W., & Pinnington, E. H. 1991, A&A, 249, 539
Brandt, J., et al. 1994, PASP, 106, 890
Calamai, A. G., Smith, P. L., & Bergeson, S. D. 1993, ApJ, 415, L59
Cardelli, J. A., & Ebbets, D. C. 1994, in Calibrating *Hubble Space Telescope*, *HST* Calibration Workshop, ed. J. C. Blades & A. J. Osmer (Baltimore: STScI), 322
Cardelli, J. A., Ebbets, D. C., & Savage, B. D. 1990, ApJ, 465, 789
———. 1993a, ApJ, 413, 401
Cardelli, J. A., Federman, S. R., Lambert, D. L., & Theodosiou, C. E. 1993b, ApJ, 416, L41
Cardelli, J. A., Mathis, J. S., Ebbets, D. C., & Savage, B. D. 1993c, ApJ, 402, L17
Cardelli, J. A., Savage, B. D., Bruhweiler, F. C., Smith, A. M., Ebbets, D. C., Sembach, K. R., & Sofia, U. J. 1991, ApJ, 377, L57
Cardelli, J. A., Sembach, K. R., & Savage, B. D. 1995, ApJ, 440, 241
Cardelli, J. A., Sofia, U. J., Savage, B. D., Keenan, F. P., & Dufton, P. L. 1994, ApJ, 420, L29
Duncan, D. K., & Ebbets, D. C. 1990, Goddard High-Resolution Spectrograph Instrument Handbook, Version 2.1 (Baltimore: STScI)
Fang, Z., Kwong, V. H. S., Wang, J., & Parkinson, W. H. 1993, Phys. Rev. A., 48, 1114
Federman, S. R., Sheffer, Y., Lambert, D. L., & Gilliland, R. L. 1993, ApJ, 413, L51
Fitzpatrick, E. L., & Spitzer, L. 1994, ApJ, 427, 232

Fuhr, J. R., Martin, G. A., & Wiese, W. L. 1988, J. Chem. Ref. Data, 17, Suppl. 4
Jenkins, E. B. 1987, in Interstellar Processes, ed. D. J. Hollenbach & H. A. Thronson (Dordrecht: Reidel)
Kurucz, R. L. 1989, unpublished
Lambert, D. L., Sheffer, Y., Gilliland, R. L., & Federman, S. R. 1994, ApJ, 420, 756
Lugger, P., Barker, E., York, D. G., & Oegerle, W. 1982, ApJ, 259, 67
Meyer, D. M., Welty, D. E., & York, D. G. 1989, ApJ, 343, L37
Meyer, D. M., & York, D. G. 1992, ApJ, 399, L21
Morton, D. C. 1991, ApJS, 77, 119
Nussbaumer, H., Pettini, M., & Storey, P. J. 1981, A&A, 26, 351
Savage, B. D., Cardelli, J. A., Bruhweiler, F. C., Smith, A. M., Ebbets, D. C., & Sembach, K. R. 1991, ApJ, 377, L53
Savage, B. D., Cardelli, J. A., & Sofia, U. J. 1992, ApJ, 401, 706
Savage, B. D., & Sembach, K. R. 1991, ApJ, 379, 245
———. 1994, ApJ, 434, 145
Shull, J. M., van Steenberg, M., & Seab, C. G. 1983, ApJ, 271, 408
Sofia, U. J., Cardelli, J. A., & Savage, B. D. 1994, ApJ, 430, 650
Sofia, U. J., Savage, B. D., & Cardelli, J. A. 1993, ApJ, 413, 251
Songaila, A., et al. 1994, Nature, 371, 43
Spitzer, L., & Fitzpatrick, E. L. 1993, ApJ, 409, 299
Steidel, C. C., Bowen, D. V., Blades, J. C., & Dickinson, M. 1995, ApJ, in press
Welty, D. E., Hobbs, L. M., & Kulkarni, V. P. 1994, ApJ, 436, 152
Wolfe, A. M., Fan, X.-M., Tytler, D., Vogt, S. S., Keane, M. J., & Lanzetta, K. M. 1994, ApJ, 435, L101